Applied Catalysis A: General 457 (2013) 26–33

Contents lists available at SciVerse ScienceDirect

Applied Catalysis A: General

journal homepage: www.elsevier.com/locate/apcata

Acid sites development on Cr^{3+}/SiO_2 catalysts obtained by the sol–gel method and hydrothermal treatment: Effect of calcination temperature

Pablo M. Cuesta Zapata [a], Mónica L. Parentis [b], Elio E. Gonzo [b], Norberto A. Bonini [c,*]

[a] INIQUI-CONICET, Avda. Bolivia 5150, 4400 Salta, Argentina
[b] INIQUI – CIUNSa – Fac. de Ingeniería, Avda. Bolivia 5150, 4400 Salta, Argentina
[c] INIQUI – CIUNSa – Fac. de Ciencias Exactas, Avda. Bolivia 5150, 4400 Salta, Argentina

ARTICLE INFO

Article history:
Received 7 December 2012
Received in revised form 20 February 2013
Accepted 27 February 2013
Available online xxx

Keywords:
Cr/SiO_2
Sol–gel
DRUV–vis
2,6-Lutidine
2-Propanol

ABSTRACT

Cr/SiO_2 catalysts (4–8% Cr, w/w), obtained from Cr(III) salts and tetraethylortosilicate (TEOS), were prepared by the sol–gel method. After TEOS hydrolysis in ammoniacal solution (pH: 9.5), the gel was treated under hydrothermal conditions at 120–220 °C. The solids were characterized by N_2 sorptometry, TG–DTA, DRUV–vis, XRD, and FTIR. In vacuum or N_2 atmosphere, Cr^{3+} ions were stable up to 450 °C. However, calcination in air promotes the partial oxidation of Cr^{3+} to Cr^{6+} as the temperature increases from 200 to 450 °C. The amount of Cr^{6+} formed depends on the temperature of the hydrothermal treatment. 2,6-Lutidine adsorption allows to determine the evolution, with respect to calcination temperature, of both Lewis and Brönsted acid centers. Cr^{3+} ions were related to the presence of Lewis sites, and Cr^{6+} ions to the development of weak Brönsted acid sites. Accordingly, the 2-propanol dehydration reaction rate shows an increase when the catalysts are treated in N_2 at 450 °C, while catalysts calcined in air develop a lower acidity. The dehydration reaction is attributed to the presence of Lewis acid centers.

1. Introduction

Chromium silica (Cr/SiO_2) catalysts have been the subject of many studies, owing to their involvement in different reactions of industrial interest. These catalysts were used in reactions such as ethylene polymerization [1–5], dehydrogenation and oxidative dehydrogenation of hydrocarbons [6–9], water gas-shift reaction [10], and the oxidation and oxydehydrogenation of alcohols and diverse organic substrata, both in gas and in liquid phase [7,8].

The Cr/SiO_2, Phillips catalyst, is responsible for more than one-third of all the polyethylene (PE) produced in the world. The Phillips catalyst has attracted the interest of academic researchers since it was patented in 1958. In these catalysts the active sites were Cr^{2+} ions anchored to the silica surface after CO or ethylene reduction of the chromate species precursors. Despite all research efforts and the recent advances they have produced [1–4], the structure of the chromate species and the coordination sphere of the active sites have not been well defined, due to both the chemical behavior of chromium and the complex structure of the amorphous silica support [5].

The catalytic conversion of alkanes into corresponding alkenes was studied using different Cr/SiO_2 catalysts [6–9]. On these materials the proposed active species were mononuclear Cr^{3+} ions anchored to the silica surface through siloxane bonds. These species can be reduced to Cr^{II} by CO, but not by H_2, at 723 K.

Takehira et al. [11] reported that only one type of chromate was formed on Cr-MCM-41 prepared under direct hydrothermal synthesis (DHT) at 423 K, and that the redox system Cr^{3+} (octahedral)/Cr^{6+} (tetrahedral) was involved in the oxidative dehydrogenation of propane. The same authors found that this catalyst showed high selectivity in the oxidation of CH_4 to HCHO [12].

In catalysts with highly dispersed chromium ions prepared both by ion exchange of mono and binuclear Cr^{3+} complexes, the alcohol dehydrogenation reaction rate was dependent on the amount of Cr^{3+} centers anchored to the support surface [13–15]. These Cr^{3+} centers developed Lewis acidity, as determined by both pyridine (Py) adsorption and by the 2-propanol dehydration reaction. This Lewis acidity was correlated to the coordinatively unsaturated Cr^{3+} ions incorporated to the silica structure. These Cr^{3+} centers were active for the oxidative dehydrogenation of alcohols in the gas phase and the ciclohexanol to ciclohexanone oxidation in the liquid phase in presence of tert-butyl hydroperoxide and O_2. In these studies the catalytic activity was attributed to chromium ions anchored

* Corresponding author. Tel.: +54 387 4251006; fax: +54 387 4251006.
E-mail addresses: pcuesta@unsa.edu.ar (P.M. Cuesta Zapata), mparentis@unsa.edu.ar (M.L. Parentis), gonzo@unsa.edu.ar (E.E. Gonzo), bonini@exa.unsa.edu.ar, bonini@unsa.edu.ar (N.A. Bonini).

0926-860X/$ – see front matter © 2013 Elsevier B.V. All rights reserved.
http://dx.doi.org/10.1016/j.apcata.2013.02.028

to the silica surface capable of producing the redox equilibrium Cr^{3+}–Cr^{6+}. It is evident that Cr^{3+} ions anchored to the SiO_2 surface and fixed to the structure through siloxane bonds are important precursors in the reversible redox system involved in these reactions.

Cr/SiO_2 catalysts were also used to catalyze the liquid phase oxidation of different substrates [16–23]. The leaching of chromium into the liquid phase seems to be a problem for Cr-containing SiO_2 materials [21]. The incorporation of Cr^{3+} ions into the support structure would be an alternative to avoid the dissolution of Cr^{6+} ions into the liquid phase. The sol–gel method followed by hydrothermal treatment is a good alternative for controlling this chromium–silica interaction.

The aim of this work is to characterize the acidic behavior of $Cr–SiO_2$ (4–8%, w/w) materials, with highly dispersed mononuclear Cr^{3+} atoms, prepared by the sol–gel method and hydrothermal treatment at 120–220 °C.

2. Experimental

2.1. Catalysts preparation

Tetraethyl ortho silicate (TEOS, Merck) was used as the silica source in all syntheses. It was mixed with ethanol (EtOH) (Merck 99.9%) and distilled water. Then, a solution of $Cr(NO_3)_3{\cdot}9H_2O$ (ANEDRA >98%) dissolved in a $EtOH/H_2O$ (1:1, v/v) mixture was dropped under stirring. The amount of chromium was the required to obtain a Cr/TEOS molar ratio of 0.06 (5SG) and 0.11 (10SG) respectively. The final mixture (molar ratio of 1.0TEOS:225.0H_2O:30.3EtOH), was vigorously stirred, the pH adjusted to 9.5 with NH_4OH (Merck), and then heated at 60 °C for 1 h and allowed to gel during 40 h. Portions of the gel were autoclaved in a Teflon vessel at different temperatures (120–220 °C) for 24 h. After hydrothermal treatment, the solid product was filtered and washed, first with water and then with an EtOH/acetone (1/1) mixture to avoid deposition of soluble chromium salts during drying. Finally, the samples were dried in air up to 110 °C. The materials were assigned as SG_{xxx}^{yyy} where xxx is the hydrotreatment temperature and yyy the temperature of calcination in air. Non-hydrotreated samples are denoted as SG_{nht}.

2.2. Characterization methods

2.2.1. Textural characterization

Specific surface area was determined with N_2, using the standard BET method based on adsorption data, in a relative pressure range (p/p_0) from 0.05 to 0.35. Pore size distribution (D_p) and pore volume (V_p) were calculated from the absorption branch of the isotherm by the BJH method.

2.2.2. X-ray diffraction (XRD)

X-ray diffraction (XRD) was carried out in a RIGAKU-DENKI D-Max IIC powder diffractometer with a Cu-Kα emission of 40 V.

2.2.3. Thermo gravimetric (TG) and differential thermal analysis (DTA)

TG–DTA were carried out in air, in a RIGAKU unit, at a heating rate of 10 °C/min. The amount of sample was 15 mg approximately.

2.2.4. Fourier transform infrared spectroscopy (FTIR)

Infrared spectroscopy studies were recorded on a BRUKER IFS 88 Fourier transform spectrophotometer (FTIR) and on a Perkin Elmer – FTIR Spectrum One equipment. For the transmission spectra the samples were diluted with KBr and pressed at 2 Tn/cm^2.

FTIR measurements of D_2O and 2,6-lutidine (Lu) adsorption were carried out over a self-supporting wafer (20 mg approximately) in a cell with KRS-5 windows that allows to perform vacuum and heating treatments "in situ". The cell was connected to a vacuum line (10^{-5} mmHg). Each sample was evacuated at different temperatures and the spectrum recorded (baseline). A gaseous adsorbent (Lu or D_2O) was introduced and left to equilibrate to its corresponding vapor pressure at room temperature (RT). The cell was evacuated and the spectra were recorded at different temperatures and times.

Difference spectra were obtained by subtracting the spectra of the pure sample (baseline spectrum) from those of the sample interacting with the adsorbed molecule after vacuum treatment. For quantitative determinations the spectra were normalized using, as internal standard, the overtones and combination bands in the 2100–1800 cm^{-1} spectral region [24].

2.2.5. UV–vis diffuse reflectance spectroscopy (DRUV–vis)

A GBC-918 equipment, with a $BaSO_4$ diffuse reflectance sphere as a reference, was used in the 350–800 nm range for the UV–vis diffuse reflectance analysis. The spectra were determined over previously grounded samples.

2.2.6. Atomic absorption spectroscopy (AAS)

Chromium loading was determined by atomic absorption (AA) after dissolving the samples with HF.

2.2.7. Determination of surface acidity – catalytic activity

Catalytic activity against 2-propanol (2-PrOH) was determined at atmospheric pressure in a Pyrex tubular gas flow reactor (internal diameter = 5 mm). The amount of catalyst varied from 50 to 100 mg (80–100 mesh). N_2 was used as carrier gas with a flow rate of 180 ml/m. 2-PrOH was vaporized in the carrier gas in order to obtain a partial pressure of 0.05 atm.

The composition of the effluents was determined with a gas chromatograph equipped with a combined column of Haye-Sept and Chromosob 102, and a thermal conductivity detector.

3. Results and discussion

3.1. Chromium loading and textural properties

Table 1 shows chromium loading (%Cr), BET surface area (S_{BET}), mean pore diameter (D_p) and pore volume (V_p) of the different materials.

The amount of chromium in the materials synthesized without hydrothermal treatment was, approximately, 20% lower than the theoretical amount which was added. This 20% of chromium was released during the washing of the samples, before drying.

The increase in the Cr/Si molar ratio from 0.06 to 0.11 in the starting solution produces, as expected, an increase in chromium loading but a large decrease in S_{BET}. So, the $5SG^{110}$ sample has a S_{BET} value three times higher than the $10SG^{110}$ material.

Table 1
Chromium content and textural properties of SG materials.

Catalyst	% Cr (w/w)	S_{BET} (m^2/g)	V_p (cm^3/g)	D_p (Å)
$5SG_{nht}^{110}$	4.07	608	0.735	42.6
$5SG_{125}^{110}$	4.35	372	n/d	n/d
$5SG_{150}^{110}$	4.39	240	0.358	18–34
$5SG_{175}^{110}$	4.88	187	0.222	18–34
$5SG_{200}^{110}$	4.79	170	0.212	23–35
$5SG_{220}^{110}$	4.13	136	0.154	19–25
$5SG_{aged}^{110}$	–	633	–	–
$10SG_{nht}^{110}$	8.10	209	0.708	85
$10SG_{125}^{110}$	8.23	159	–	–
$10SG_{150}^{110}$	–	136	0.503	90
$10SG_{200}^{110}$	8.76	124	–	–
$10SG_{220}^{110}$	8.10	116	0.471	81

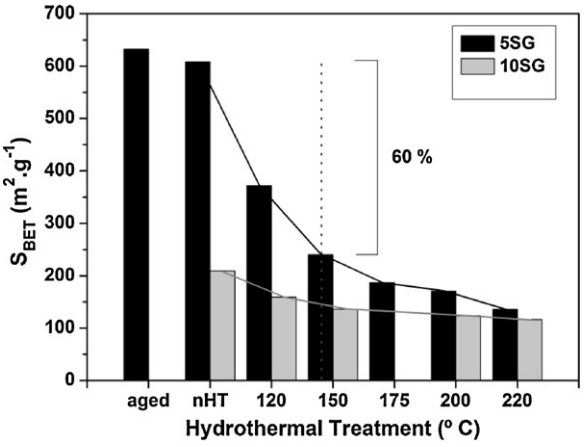

Fig. 1. Variation of the BET surface area with hydrothermal treatment.

A progressive decrease of S_{BET} as the temperature of the hydrothermal treatment increases was also observed (Fig. 1). As a result, S_{BET} decreased 60% when the sample was hydrotreated up to 150 °C while between 150 °C and 220 °C the S_{BET} drop was only 20%. This behavior is in agreement with a decrease of pore volume and mean pore diameter.

Catalysts without thermal treatment (SG^{110}) had the higher pore volume, but it decreased as the temperature of the hydrothermal treatment increased. In all cases, a broad pore size distribution was observed showing the usual pore distribution of an amorphous–siliceous material.

3.2. X-ray diffraction

For 5SG materials, XRD shows the absence of crystalline species, even after calcination in air up to 450 °C. On the contrary, all 10SG materials show the development of cristalline α-Cr_2O_3 difraction lines after calcination in air up to 280 °C for 24 h (Fig. 2).

The absence of diffraction lines typical of crystalline compounds in the 5SG samples, both calcined and uncalcined, shows the high dispersion of chromium. Conversely, the development of cristaline α-Cr_2O_3 in 10SG samples is directly related to the higher amount of chromium, as well as to lower S_{BET} areas. This α-Cr_2O_3, more stable thermodinamically, is formed during calcination from segregated CrO_3.

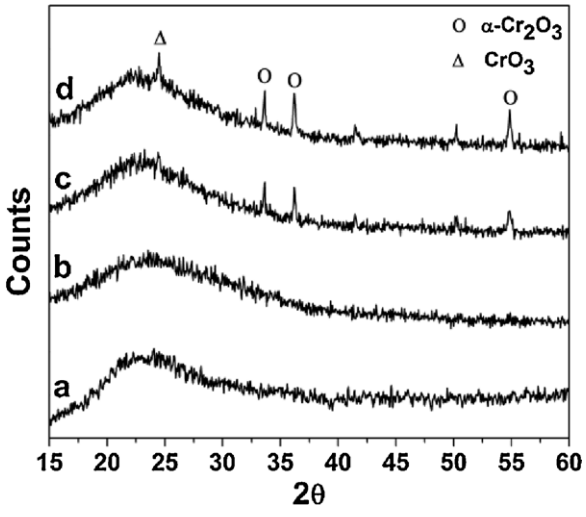

Fig. 2. XRD of $10SG_{220}$ sample after different thermal treatments in air: (a) $10SG_{220}{}^{110}$; (b) $10SG_{220}{}^{180}$; (c) $10SG_{220}{}^{280}$; (d) $10SG_{220}{}^{450}$.

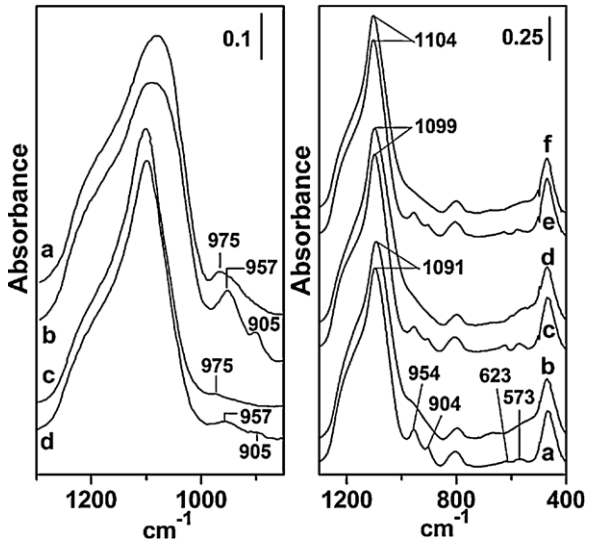

Fig. 3. Left – FTIR spectra of 5SG samples calcined at different temperatures: (a) $5SG_{nht}{}^{110}$; (b) $5SG_{nht}{}^{450}$; (c) $5SG_{220}{}^{110}$; (d) $5SG_{220}{}^{450}$. Right – FTIR spectra of 10SG samples: (a) $10SG_{nht}{}^{450}$; (b) $10SG_{nht}{}^{110}$; (c) $10SG_{150}{}^{450}$; (d) $10SG_{150}{}^{110}$; (e) $10SG_{220}{}^{450}$; (f) $10SG_{220}{}^{110}$.

In all samples, centered around $2\theta \approx 22$, a broad band characteristic of amorphous silica was observed.

3.3. Fourier transform infrared spectroscopy (FTIR)

Fig. 3 shows the FTIR spectra of KBr diluted wafers of catalysts calcined in air at different temperatures. All materials developed bands at 470, 805, 975 and 1100 cm^{-1}; the last band with a shoulder at 1200 cm^{-1}.

The band at 470 cm^{-1} is assigned to the ρ(Si—O—Si) bending mode, while bands centered at 805 cm^{-1}, together with the broad band with a shoulder at 1100 cm^{-1}, correspond to the symmetric ν_s(Si—O—Si) and asymmetric ν_{as}(Si—O—Si) stretching modes of the SiO_4 tetrahedra of silica structure.

The broadening of the band at 1100 cm^{-1}, and its location at frequencies lower than 1100 cm^{-1}, reflects the heterogeneity of the Si—O—Si bonds characteristic of an amorphous silica structure. The band at 975 cm^{-1} has been assigned to the Si—O bond vibration of the superficial hydroxyl groups; it decreases in intensity with hydrothermal treatment (Fig. 3a). The decrease in the intensity of this band, when hydrotreatment temperature increases, is related both to the formation of Si—OCr bonds and to the drop of S_{BET}.

The effect of hydrothermal treatment is to redisolve the amorphous silica in order to develop a more uniform and ordered support structure. This effect, more evident as the hydrotreatment temperature increases, causes the ν_{as}(Si—O—Si) band to shift to higher frecuencies, from 1090 to 1106 cm^{-1}, and a decrease in the band width (FWHM).

All samples calcined at 450 °C developed two bands around 905 and 955 cm^{-1}. These bands are characteristic of oxidized species of Cr^{6+}. They are assigned to symmetric and asymmetric stretching modes of O═Cr═O bonds present in chromates, dichromates and CrO_3 oxide [13,14]. The intensity of these bands depends on chromium loading and on the temperature of the hydrothermal treatment. So, whereas the $5SG_{nht}{}^{450}$ sample developed two intense bands at 957 and 905 cm^{-1} after 450 °C calcination (Fig. 3 – left (a) and (b)), the intensity of these bands diminished on the $5SG_{220}{}^{450}$ sample (Fig. 3 – left (c) and (d)). The resistance to form Cr^{6+} species as the temperature of hydrotreatment increases is assignable to a higher interaction of Cr^{3+} with the support.

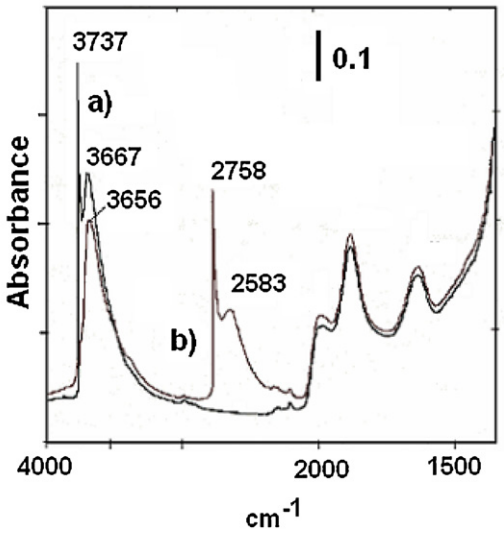

Fig. 4. Deuterium exchange over $5SG_{220}{}^{110}$ catalyst. (a) $5SG_{220}{}^{110}$ evacuated at 460 °C by 1 h. (b) D_2O vapor in contact with the sample and after evacuation at RT for 30 min.

The absence of diffraction lines on 5SG samples, corresponding to crystaline species of Cr^{6+}, demonstrates the high dispersion of the Cr^{6+} oxides. It leads to the formation of surface chromates as reported by other autors [2,4,13,14].

On the 10% chromium loading materials, calcination in air induces Cr^{6+} oxide formation. However, a fraction is segregated and transformed to crystalline α-cromia. Cr_2O_3 formation was confirmed on these materials both by XRD (Fig. 2) and by its characteristic bands at 623 and 573 cm^{-1} in the FTIR spectra (Fig. 3 – right a–f).

3.4. Vacuum treatment and deuterium exchange

FTIR spectra of samples in the region between 3750 and 3000 cm^{-1}, after vacuum treatment at 10^{-5} mmHg (Fig. 4a), show two bands at 3737 and 3667 cm^{-1} that reveal the presence of different types of hydroxyl groups resistant to evacuation up to 450 °C. The first one corresponds to Si—OH isolated groups.

After deuterium exchange, the spectrum shows two new bands at 2758 and 2583 cm^{-1} assigned to stretching frequencies of O—D bonds and to the disappearance of the 3737 cm^{-1} band. Accordingly, the band at 3667 cm^{-1} shifts to 3656 cm^{-1}. This band is more intense and sharper, as the severity of hydrothermal treatment increases from 120 to 220 °C. It remains after D_2O exchange, which demonstrates its occlusion. This band cannot be assigned to superficial, germinal or vicinal, Si—OH groups because in amorphous silica these groups are not only exposed to deuterium exchange but they are also almost completely removed at 450 °C. Therefore, the band at 3656 cm^{-1} must be associated to the presence of chromium ions and assigned to the incipient formation of hydrosilicate structure [8,10]. These results are congruent with those previously observed by DRX and FTIR. Thus, as the hydrothermal temperature increases, the amount of chromium forming SiO—Cr bonds increases.

Besides, samples treated in vacuum at 350 °C show the presence of two bands, as shoulders, at 3250 and 3180 cm^{-1}, which are assignable to the stretching vibration of N—H bonds of ammonia present in the catalyst as chromium ligands [14]. These bands remain as a trace up to 450° in vacuum (Fig. 4). Regardless of their resistance in vacuum, heating in air at 150 °C produces the total loss of these bands.

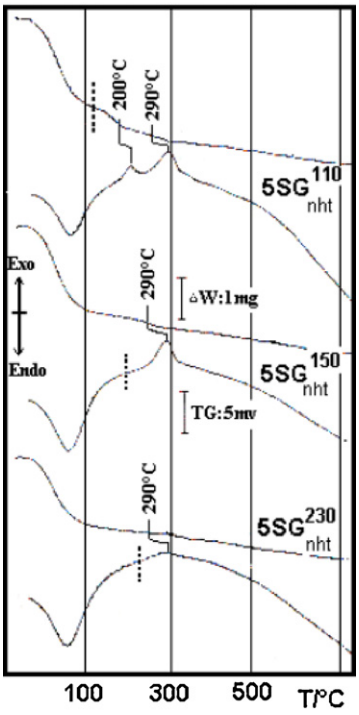

Fig. 5. TG–DTA measurements on $5SG_{nht}$ sample. Vertical dotted lines in the DTA curves represent the temperature of calcination in air of the samples (see the text).

3.5. TG and DTA analysis

Calcination in air at different temperatures induces color changes that are consistent with the loss of ligands and with changes in the chromium oxidation state.

Thus, the non-hydrotreated samples dried in air at 110 °C showed a green color characteristic of the Cr(III) hydrated ion. In air, it went through a dark green color near 150 °C, then to a reddish brown at 220 °C and finally became orange-yellow, the characteristic color of chromium (VI) oxides, at 450 °C. These changes were accompanied by exothermic and endothermic transformations with consequent loss of weight observed by TG–DTA measurements (Fig. 5).

All catalysts develop, at between 70 °C and 150 °C, an endothermic band and an important loss of weight due to the elimination of physically adsorbed water. After that, a continuous loss of weight was observed, which is assigned to water molecules released by condensation of silanol groups present at the silica surface. The total loss of weight was higher for non-hydrothermally treated samples and it decreased as the S_{BET} of the samples decreased.

The catalyst dried in air at 110 °C presents, besides this endothermic water release, two exothermic peaks. The first one centered at 200 °C (T_1) and the second at 290 °C (T_2), both with loss of weight. Calcination of $5SG_{nht}{}^{110}$ material in air during 24 h up to 150 °C ($5SG^{150}$) causes the disappearance of the first exothermic peak, while calcination at 230 °C causes the almost disappearance of the last one.

The first exothermic peak at 200 °C (T_1) is assigned to the formation of Cr^{3+}—OSi bonds. These bounded chromium species are oxidized to Cr^{6+} at 290 °C (T_2) with the formation of monochromate. Evidence of these chromium oxidized species was confirmed by the presence of bands at 957 and 905 cm^{-1} (Fig. 3).

Hydrothermal treatment causes the disappearance of the first exothermic peak (T_1 = 200 °C) and the gradual decrease in intensity of the second one (T_2). Therefore, the T_2 peak is not only almost absent in the $5SG_{220}{}^{110}$ sample but it shifts toward 340 °C. This

Table 2
Electronic transitions of Cr^{3+} ions observed by DRUV–vis spectroscopy.

Allowed electronic transitions for the d^3 ion Cr^{3+} $(H_2O)_6$ [25]		
$^4T_{2g}(F)\cdots{}^4A_{2g}(F)$	580 nm	
$^4T_{1g}(F)\cdots{}^4A_{2g}(F)$	412 nm	
$^4T_{1g}(P)\cdots{}^4A_{2g}(F)$	260 nm	
	$^4T_{2g}(F)\cdots{}^4A_{2g}(F)$	$^4T_{1g}(F)\cdots{}^4A_{2g}(F)$
Electronic transitions (nm) observed on hydrothermal treated materials		
$5SG_{nht}{}^{110}$	610	425
$5SG_{125}{}^{110}$	612	432
$5SG_{150}{}^{110}$	622	438
$5SG_{175}{}^{110}$	625	440
$5SG_{200}{}^{110}$	630	442
$5Sg_{220}{}^{110}$	635	444
	$^4T_{2g}(F)\cdots{}^4A_{2g}(F)/{}^4T_{1g}(F)\cdots{}^4A_{2g}(F)$	
Intensity ratio in the visible–absortion bands of different 5SG materials		
$5SG_{nht}{}^{110}$	1.00	
$5Sg_{125}{}^{110}$	1.33	
$5Sg_{150}{}^{110}$	1.65	
$5SG_{175}{}^{110}$	1.72	
$5SG_{200}{}^{110}$	1.77	
$5Sg_{220}{}^{110}$	2.00	

behavior reflects an improvement of Cr^{3+} interaction with the silica structure, promoting Cr^{3+}—OSi bond formation.

An exothermic peak at a temperature above 550 °C, indicating the formation of α-Cr_2O_3, was observed in all 10SG materials.

3.6. UV–vis diffuse reflectance spectroscopy (DRUV–vis)

The analysis of samples by DRUV–vis confirms these findings. Cr^{3+} is a d^3 ion that presents three intense absorption bands, in the 200–900 nm spectral region, corresponding to three allowed electronic transitions (Table 2). The $[Cr(H_2O)_6]^{3+}$ ion shows these bands centered at 580, 412 and 260 nm, and also a weak band as a shoulder at 680 nm corresponding to a spin-forbidden transition [25]. The $5SG_{nht}{}^{110}$ material shows a shift of the 580 and 412 nm bands toward higher wavelengths at 610 and 425 cm^{-1} respectively. This red shift is due to the presence of ammonia as ligand and the incorporation of Si—O— groups in the outer coordination sphere of Cr^{3+} ions. The presence of ammonia as ligand was confirmed by FTIR spectra of samples, as was previously discussed. On the other hand, calcination in air at 150 °C results in the elimination of ammonia and the formation of Si—O—Cr bonds.

In agreement with this behavior, the DRUV–vis spectra of this material, first treated in air at 150 °C and then at 230 °C during 24 h (Fig. 6) display a gradual shift of the 610 cm^{-1} band toward higher wavelengths with the almost disappearance of the characteristic d^3 electronic structure. Further calcination in air at 450 °C produces a

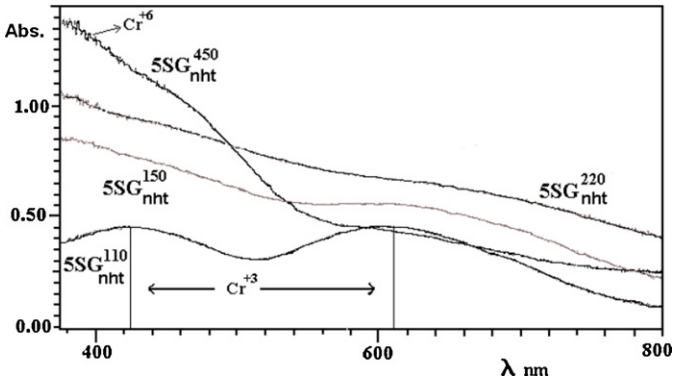

Fig. 6. DRUV–vis spectra of $5SG_{nht}$ samples after different calcination temperatures.

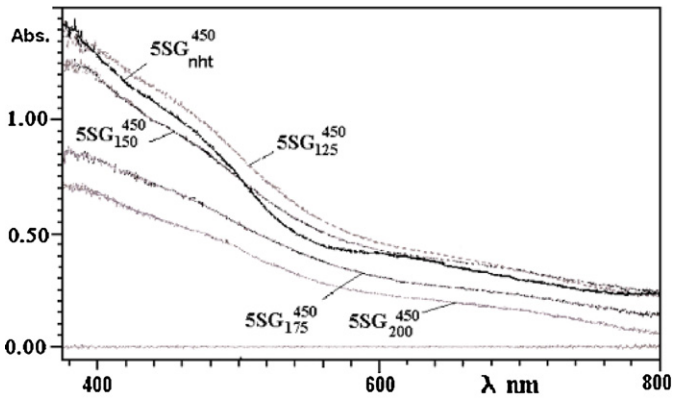

Fig. 7. DRUV–vis spectra of samples prepared under different hydrothermal conditions after calcination up to 450°.

spectrum corresponding to Cr^{6+}. It is easily identified by the very intense absorption band at 380 nm, assigned to a ligand to metal charge transfer band (LMCT) [2,21].

The development of a week band centered at 610 nm probably corresponds to a small amount of α-Cr_2O_3 formed after Cr^{6+} oxide segregation. As the temperature of the hydrothermal treatment increases the spectra of samples calcined in air up to 450 °C show a higher resistance of Cr^{3+} to Cr^{6+} oxidation (Fig. 7). So, while the $5SG_{nht}{}^{450}$ sample displayed a strong absorption band at 380 nm due to the formation of Cr^{6+} species, a gradual decrease in the intensity of the LMCT band was observed as the temperature of the hydrothermal treatment increased. Finally, the $5SG_{220}{}^{450}$ catalyst shows a DRUV–vis spectrum corresponding to a material containing a mixture of chromium species, some of them probably in an intermediate oxidation state.

A shift of the bands toward higher wavelengths due to the effect produced by hydrothermal-treatment was also observed (Fig. 8 and Table 2). Thus, a gradual increase of the hydrotreatment temperature during the synthesis produces a gradual shift in the $^4T_{2g}(F)$—$^4A_{2g}(F)$ absorption band, from 610 nm ($5SG^{110}$) to 635 nm. This behavior must be justified by the formation of Si—O—Cr bonds. The shift was accompanied by a strong change in the relative intensities of the absorption bands. As a result, the ratio $R = (^4T_{2g}\cdots{}^4A_{2g})/(^4T_{1g}\cdots{}^4A_{2g})$ goes from 1, for $5SG_{nht}{}^{110}$, to 2 for $5SG_{220}{}^{110}$ (Table 2 and Fig. 8). This change reflects the distortion of the octahedral field produced by the incorporation of Cr^{3+} ions in the tetrahedral structure of silica. This distortion is related to the

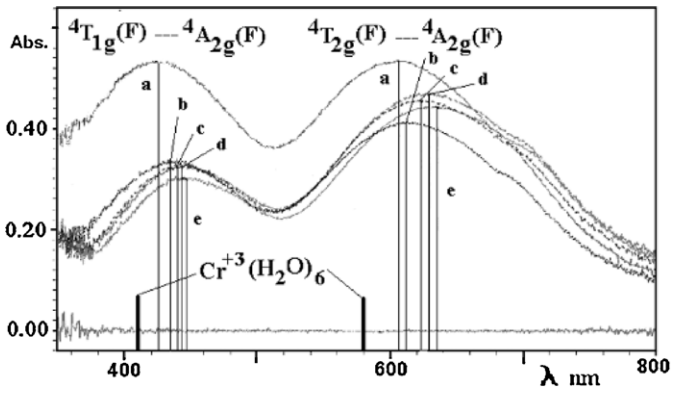

Fig. 8. DRUV–vis spectra obtained from samples prepared under different hydrothermal conditions: (a) $5SG_{nht}{}^{110}$; (b) $5SG_{125}{}^{110}$; (c) $5SG_{175}{}^{110}$; (d) $5SG_{200}{}^{110}$; (e) $5SG_{220}{}^{110}$. The shoulder between 680 and 710 nm corresponds to a spin-forbidden transition.

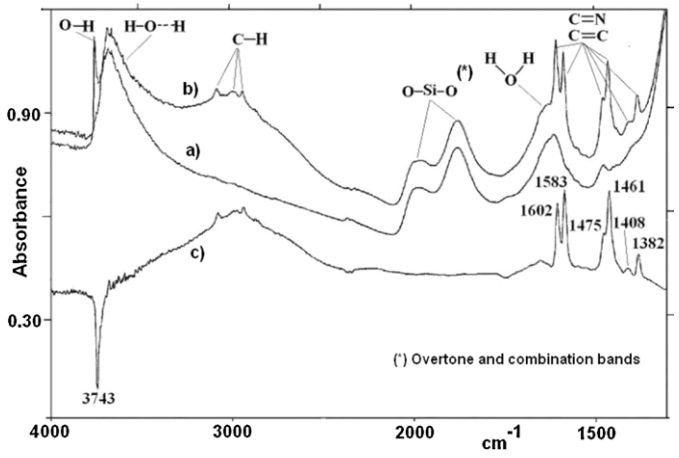

Fig. 9. FTIR spectra of L-Lu and H_B-Lu: (a) $5SG_{nht}{}^{110}$ sample evacuated at 250 °C; (b) Lu adsorbed at RT after vacuum at 50 °C (1 h – 10^{-3} mmHg); (c) difference spectra b–a. The spectra were normalized using the overtone and combination bands in the 2000–1800 cm^{-1} region [24].

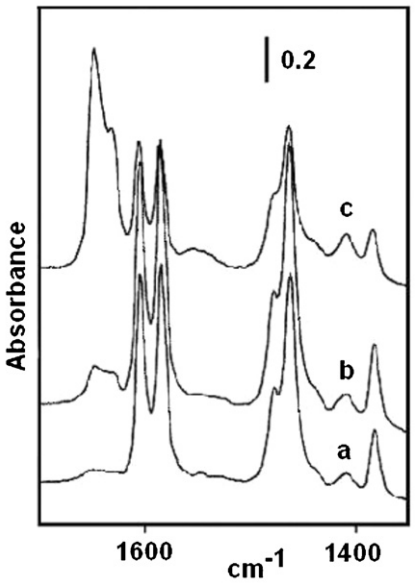

Fig. 10. Left: Lu adsorbed on $5SG_{nht}$ material after different calcination temperatures: (a) 150°; (b) 350 °C; (c) 450 °C.

formation of more strained chromium siloxane rings, as reported in the literature [2,3].

3.7. FTIR study of 2,6-lutidine adsorption

In a previous paper we reported that in the Cr/SiO_2 system the presence of chromium in different oxidation states produces the appearance of different acid centers [14]. So, the presence of Cr^{3+} anchored to the silica surface produces Lewis acid centers, the number of which increases as the amount of Cr^{3+}, incorporated to the structure of the support, increases. Furthermore, calcination in air promotes the development of weak Brönsted sites. The evolution of these acid centers can be visualized by FTIR through the adsorption of pyridine (Py) and/or 2,6-lutidine (Lu) molecules.

Py absorption on materials prepared by the SG method, without hydrotreatment, showed [14] the presence of a significant amount of Lewis (LPy) centers characterized by bands at 1612, 1489 and 1450 cm^{-1}. Only small amounts of Py associated to Brönsted centers (BPy) with bands at 1489, 1545 and 1625 cm^{-1} were observed. The LPy was resistant to evacuation at 100 °C while, the BPy was easily removed. The calcination of the samples in air lead to the appearance of weak Brönsted centers associated to the presence of Cr^{6+}.

The adsorption of Lu (conjugated acid $pK_a = 6.6$), a molecule with higher basicity than Py (conjugated acid $pK_a = 5.25$), allows for a better study of weak acid centers. When the Lu molecule interacts with an acid surface it develops strong bands in the 1550–1650 cm^{-1} spectral range (8a–8b ring stretching modes). According to their position, it is possible to discriminate among Lewis and Brönsted acid sites. Thus, bands at $\nu > 1620\ cm^{-1}$ indicate Brönsted acidity while bands in the 1580–1610 spectral region point to the existence of Lewis and/or hydrogen bonded Lu. Another group of bands, lying in the 1400–1480 cm^{-1} spectral range (19a and 19b ring stretching modes), undergo little spectral changes and are less useful.

On $5SG_{nht}{}^{110}$ materials previously evacuated at 250 °C, the Lu adsorption leads to the development of bands at 1602, 1583, 1475, 1461, 1408 and 1382 cm^{-1} (Fig. 9). These bands are assignable to hydrogen bonded lutidine (H_BLu) and/or Lu interacting with Lewis acid sites (LLu). Discriminating between them is possible only by vacuum treatment. So, while H_BLu is completely removed at 50 °C in vacuum, removing LLu requires vacuum treatment at 100 °C. When the samples were heated in N_2 or in vacuum up to 480 °C before the adsorption of Lu, the nature of the adsorbed species did not change.

The adsorption of Lu on materials calcined in air without hydrotreatment leads to the development of a band at 1644 cm^{-1} with a shoulder at 1629 cm^{-1} (Fig. 10). These bands are assignable to the appearance of a protonated 2,6-lutidinium ion, formed by reaction of Lu with Brönsted acid sites. The amount of Brönsted Lutidine (BLu) depends on both the previous hydrothermal treatment and the temperature of calcination in air. The rise in the calcination temperature increased the amount of BLu at expense of Lewis species. Therefore, on materials calcined at 450 °C the most intense band observed corresponds to BLu (Fig. 10c). These BLu species were resistant to vacuum treatment up to 100 °C. From these results we conclude that LLu is related to Cr^{3+} ions, while BLu appears when Cr^{6+} is formed by the calcination in air.

The relative amount of Brönsted and Lewis acid centers on samples with hydrothermal treatment ($5SG_{220}{}^{450}$) is markedly lower than in non-hydrothermally treated materials ($5SG_{nht}{}^{450}$) (Fig. 11). The fall in the amount of Brönsted centers coincides with a greater resistance toward oxidation of Cr^{3+} ions on hydrothermically treated samples, as was previously discussed.

To verify whether the Brönsted centers were related to the Cr^{6+} presence, a sample of $5SG_{220}{}^{450}$, which after calcination in air developed a light yellow color, was washed with acetone and ethanol. After washing, it was dried in air at room temperature, made a self supported wafer and evacuated at 150 °C into the FTIR cell. Fig. 12a shows that only LLu/H_BLu bands formed on this material after interaction with Lu.

These results let us conclude that the development of Brönsted centers is directly related to the Cr^{6+} species formed during calcination in air. Heating the washed sample in air at 450 °C (Fig. 12b) shows the formation of new Brönsted acid centers.

Conversely, the intensity of the BLu bands decreased when the sample, before the adsorption of Lu, was treated in vacuum at increasingly higher temperatures (Fig. 12c and d). The color of the sample turns progressively to dark blue-green instead of the yellow color observed on the oxidized one. So, in vacuum at 450 °C, almost all Cr^{6+} transforms to Cr^{3+}. This behavior shows that the Cr^{3+}–Cr^{6+} redox process on the Cr/SiO_2 system is reversible.

The amount of both ions depends on the temperature and the oxidative character of the atmosphere used during calcination.

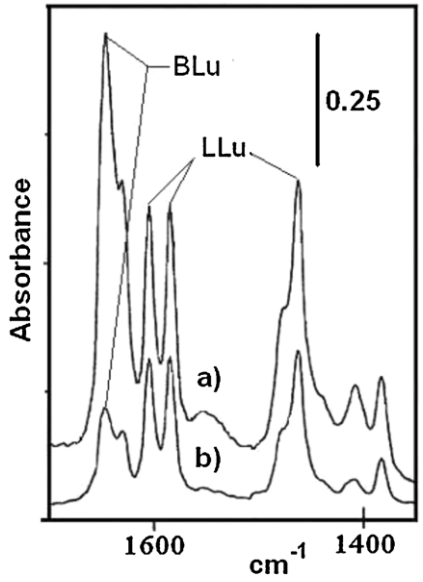

Fig. 11. BLu species developed over different 5SG materials calcined at 450 °C. (a) $5SG_{nht}^{450}$; (b) $5SG_{220}^{450}$. The spectra were determined after evacuation for 30 min at room temperature.

3.8. Catalytic activity against 2-propanol

With the aim of correlating the structural changes observed with the acidic surface properties, a study of the catalytic activity of the 2-propanol (2-PrOH) reaction (dehydration/dehydrogenation) was carried out under an N_2 atmosphere. This alcohol molecule allows evaluating the acid properties of a solid by analyzing its capacity to produce different products. So, the formation of propene and/or isopropyl ether is directly related to the presence of acid centers; while the production of 2-propanone takes place through a concerted mechanism involving both acid and basic sites [26]. The only products detected in our reaction system were acetone and propene.

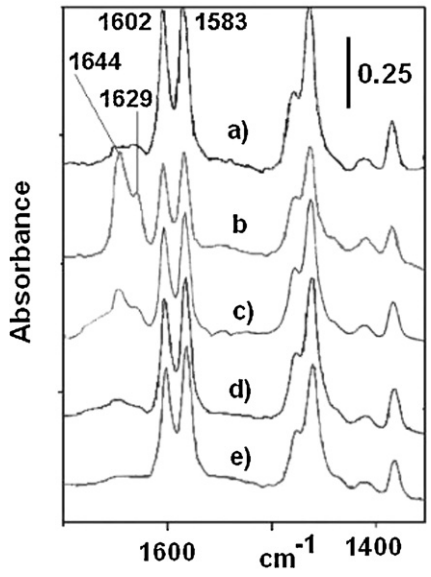

Fig. 12. Lu adsorption on $5SG_{220}^{450}$ materials after different treatments: (a) $5SG_{220}^{450}$ washed with Ac/EtOH; (b) sample (a) calcined in air up to 450 °C; (c–e) Lu adsorption on sample (b) treated in vacuum (1 h – 10^{-3} mmHg) at 250 °C, 350 and 450 °C successively. All the spectra are normalized with the 1800–2100 cm^{-1} bands.

Fig. 13 shows the changes in the reaction rate for 2-PrOH dehydration at 280 °C. This figure shows the behavior of catalysts prepared either with or without hydrothermal treatment with respect to the temperature of calcination. It can be seen that for materials dried at 110 °C the hydrothermal treatment increases the surface acidity. The incorporation of Cr^{3+} on the support promotes the formation of coordinative unsaturated (cus) centers [27] that catalyze the 2-PrOH dehydration. This behavior is observed both for 5SG and 10SG materials (Fig. 13). Selectivity toward dehydration reaction is above 95% for materials with hydrotreatment, but it is reduced by the formation of acetone in those materials which were not hydrothermally treated.

In contrast, materials with strong hydrothermal treatment ($5SG_{220}$ and $10SG_{220}$) increase their surface acidity (i.e. propene formation) as the calcination temperature increases, passing through a maximum between 250 °C and 350 °C. Calcination in air at temperatures higher than 350 °C promotes not only the oxidation of chromium but also its partial segregation; consequently, acidity diminishes. This behavior is enhanced when the samples are calcined in O_2 (Fig. 13 – left).

Conversely, samples calcined in N_2 at 450 °C did not show this decrease in acidity, maintaining the selectivity toward the formation of propene higher than 95%. In this condition, Cr^{6+} is not formed and the catalyst develops only Cr^{3+} unsaturated centers. In all cases, hydrothermally treated samples at higher temperatures ($5SG_{220}$ and $10SG_{220}$) exhibited higher values of selectivity toward the production of propene.

The $10SG_{150}$ catalyst (Fig. 13 – right) shows intermediate propene reaction rates and selectivity between those observed on $10SG_{nht}$ and $10SG_{220}$ materials.

The activation energy for the dehydration reaction remained almost invariant (15 ± 2 kcal/mol) in the materials calcined up to 350 °C but showed a little increase up to 20 kcal/mol for materials calcined at 450 °C, both in air or O_2. This behavior shows that the variation in acidity is primarily due to a change in the amount or eventually the strength, of the acid centers, but not to a change in their nature (Lewis or Brønsted).

The maximum acidity produced by calcination temperature resembles an activation process that promotes the formation of different chromasiloxane rings whose strain is related to the size of the ring [2]. Demmelmaier et al. [3] pointed out that strained six-member rings, which are more abundant on catalysts pretreated at higher temperatures, develop higher ethylene polymerization activities, probably due to their high insaturation [2,3]. A similar behavior was reported by Takehira et al. for materials prepared by direct hydrothermal synthesis (DHT) at 423 K [11].

According to what has been previously discussed, there is an ample agreement with that determined from the different techniques of characterization employed (XRD, FTIR, TG–DTA, DRUV–vis among others). So, the increase of the temperature of hydrotreatment produces an increase in the amount of Cr^{3+} incorporated to the support. This promotes a greater resistance against the formation of Cr^{6+} oxidized species when samples are calcined in air. The Cr^{3+}/Cr^{6+} ratio depends on the calcination temperature, the chromium loading and the temperature of the hydrotreatment.

The grafted Cr^{3+} species induce the appearance of Lewis acids centers due to the development of coordinatively unsaturated (cus) sites. The calcination in air of these materials oxidizes a fraction of Cr^{3+} ions, which gives rise the formation of Brønsted acids sites. They differentiate from Lewis sites by the adsorption of 2,6-lutidine. These Brønsted sites disappear by washing with acetone/ethanol mixture; besides, they are reduced to Cr^{3+} by treatment in vacuum up to 450 °C.

According to the bibliography [26], neither amorphous silica nor α-Cr_2O_3 shows an acidic behavior against 2-propanol in the 180–270 °C temperature range. On the contrary, on SG materials

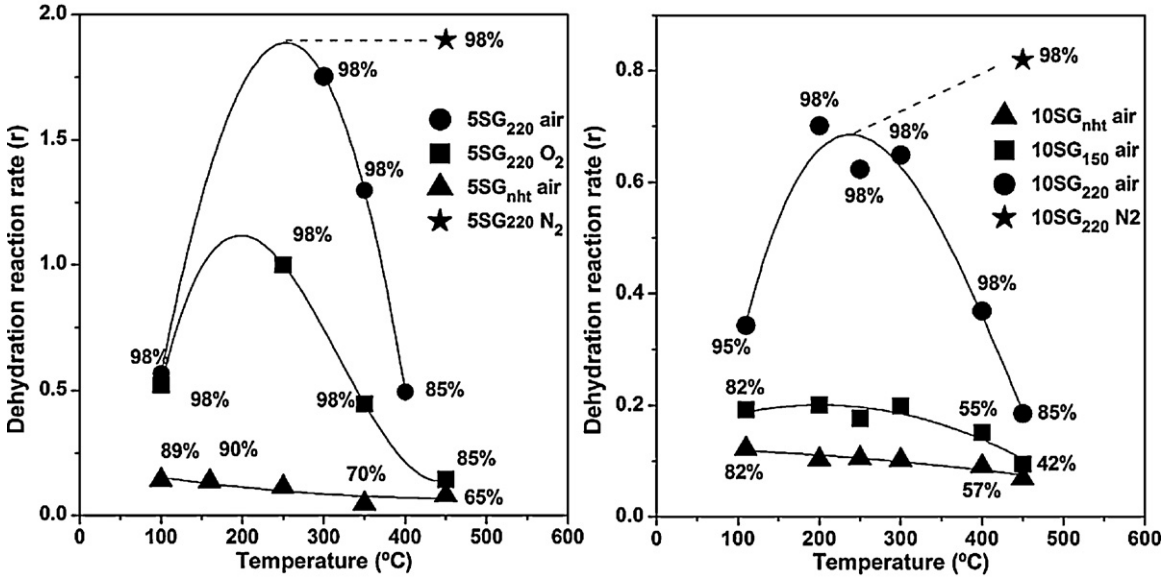

Fig. 13. Variation of the 2-Prol dehydration reaction rate (r = mol propene/(h.mol Cr. S_{BET})) at 280 °C vs. calcination temperature for different materials. The percent numbers in the graphic are the selectivities to propene.

the 2-PrOH reaction at 280 °C shows a distinctly acid behavior with high selectivity toward the formation of propene. The dehydration reaction rate is higher on hydrotreated samples. The increase of calcination temperature increases the acidity of these materials, passing through a maximum and finally decreasing as Cr^{6+} is formed. This maximum of acidity is justified by the formation of Cr^{3+}, cus ions, the unsaturation of which increases when the calcination temperature increases up to 350 °C.

The decrease in the dehydration reaction rate after the calcination in air up to 450 °C coincides with a decrease in selectivity by the formation of acetone. This behavior is common for all materials in which the formation of Cr^{6+} is favored. This is justifiable, considering that the dehydrogenation reaction requires the simultaneous presence of acidic and basic sites [26]. Thus, the materials without hydrotreatment ($5SG_{nht}$ and $10SG_{nht}$) show a lower selectivity to dehydration products.

4. Conclusions

Cr/SiO_2 materials prepared by the sol–gel method, combined with an hydrothermal treatment between 150 °C and 220 °C, enable to make catalysts where Cr^{3+} ions are incorporated into the silica structure through the formation of SiO—Cr^{3+} bonds. These Cr^{3+} ions are incorporated to chromasiloxane rings developing Lewis acid sites whose strength increases as calcination temperature increases up to 350 °C. These sites, highly unsaturated, are responsible for the dehydration reaction. A fraction of these sites is oxidized to Cr^{6+} when the materials are heated in air or oxygen, producing weak Brönsted acid sites. Both, Lewis and Brönsted acid sites can be monitored through the adsorption of 2,6-lutidine. The amount of Cr^{6+} formed depends on the temperature of the hydrothermal treatment. These sites are able produce a reversible redox, Cr^{3+}/Cr^{6+} system. The resistance to segregation of Cr^{6+} ions depends on chromium loading, hydrothermal treatment temperature, calcinations temperature and oxidant conditions.

Acknowledgments

This work was performed under the auspices and the financial support of INIQUI-CONICET and CIUNSa.

References

[1] B.M. Weckhuysen, I.E. Wachs, R.A. Shoonheydt, Chem. Rev. 96 (1996) 3327–3350.
[2] E. Groppo, C. Lamberti, S. Bordiga, G. Spoto, A. Zecchina, Chem. Rev. 105 (2005) 115–183.
[3] C.A. Demmelmaier, R.E. White, J.A. van Bokhoven, S.L. Scott, J. Catal. 262 (2009) 443–456.
[4] M.P. McDaniel, Adv. Catal. 53 (2010) 123–606.
[5] A. Zecchina, E. Groppo, Proc. R. Soc. A 468 (2143) (2012) 2087–2098.
[6] G.S. Pozan, A. Tavman, I. Boz, Chem. Eng. J. 143 (2008) 180–185.
[7] J. Santamaría-González, J. Mérida-Roblea, M. Alcántara-Rodríguez, P. Maireles-Torres, E. Rodríguez-Castellón, A. Jiménez-López, Catal. Lett. 64 (2000) 209–214.
[8] S. De Rossi, M.P. Cansaletto, G. Ferraris, A. Cimino, G. Minelli, Appl. Catal. A: Gen. 167 (1998) 27–270.
[9] S. De Rossi, G. Ferraris, S. Fremiotti, E. Garrone, G. Ghiotti, M.C. Campa, V. Indovina, J. Catal. 148 (1994) 36–46.
[10] W.K. Józwiak, W. Ignaczak, D. Dominiak, T.P. Maniecki, Appl. Catal. A: Gen. 258 (2004) 33–45.
[11] K. Takehira, Y. Ohishi, T. Shishido, T. Kawabata, K. Takaki, Q. Zhang, Y. Wang, J. Catal. 224 (2004) 404–416.
[12] Y. Wang, Y. Ohishi, T. Shishido, Q. Zhang, W. Yang, Q. Guo, H. Wang, K. Takehira, J. Catal. 220 (2003) 347–357.
[13] M. Parentis, N. Bonini, E.E. Gonzo, Latin Am. Appl. Res. 32 (2002) 41–46.
[14] M.L. Parentis, N.A. Bonini, E.E. Gonzo, Latin Am. Appl. Res. 30 (2000) 41–50.
[15] M.L. Parentis, N.A. Bonini, E.E. Gonzo, React. Kinet. Catal. Lett. 72 (2) (2001) 303–308.
[16] P. Brandao, A. Valente, A. Ferreira, V. Amaral, J. Rocha, Microporous Mesoporous Mater. 69 (3) (2004) 209–215.
[17] M.E. González-Núñez, R. Mello, A. Olmos, R. Acerete, G. Asensio, J. Org. Chem. 71 (2006) 1039–1042.
[18] R.A. Shaikh, G. Chandrasekar, K. Biswas, J. Choi, W. Son, S. Jeong, W. Ahn, Catal. Today 132 (2008) 52–57.
[19] S. Samanta, N.K. Mal, A. Bhaumik, J. Mol. Catal. A. Chem. 236 (2005) 7–11.
[20] S.K. Mohapatra, P. Selvam, J. Catal. 249 (2007) 394–396.
[21] A. Sakthivel, S.E. Dapurkar, P. Selvam, Appl. Catal. A: Gen. 246 (2003) 283–293.
[22] H. Liu, Z. Wang, H. Hu, Y. Liang, M. Wang, J. Solid State Chem. 182 (2009) 1726–1732.
[23] S.C. Laha, R. Kumar, Microporous Mesoporous Mater. 53 (2002) 163–167.
[24] R. Buzzoni, S. Bordiga, G. Ricchiardi, C. Lamberti, A. Zecchina, G. Bellussi, Langmuir 12 (4) (1996) 930–940.
[25] J.E. Huheey, E.A. Keiter, R.L. Keiter, Ianorganic Chemistry: Principles of Structure and Reactivity, fourth ed., Harper Collins, New York, 1993.
[26] A. Gervasini, A. Auroux, J. Catal. 131 (1991) 190–198.
[27] G. Conell, J.A. Dumesic, J. Catal. 105 (2) (1987) 285–298.